Spin Fluctuations of Paramagnetic Rh Clusters Revealed by X-Ray Magnetic Circular Dichroism

V. M. T. S. Barthem,[1] A. Rogalev,[2] F. Wilhelm,[2] M. M. Sant'Anna,[1] S. L. A. Mello,[1] Y. Zhang,[3] P. Bayle-Guillemaud,[4] and D. Givord[1,3]

[1]*Instituto de Física, Universidade Federal do Rio de Janeiro, 21941-972 Rio de Janeiro, Brazil*
[2]*European Synchrotron Radiation Facility, BP 220, F-38043 Grenoble, France*
[3]*Institut Néel, CNRS/UJF, BP 166, 38042 Grenoble cedex 9, France*
[4]*CEA-INAC/UJF, SP2M, LEMMA, Minatec Grenoble, F-38054, France*

(Received 15 March 2012; published 9 November 2012)

The magnetic moment induced on Rh atoms, forming 1.6 nm average diameter clusters, embedded in an Al_2O_3 matrix, has been determined using x-ray magnetic circular dichroism measurements. The magnetic moment varies linearly with the applied magnetic field. At 2.3 K and under 17 T, the spin magnetic moment amounts to 0.067(2) μ_B/Rh atom. The orbital moment does not exceed 2% of the spin moment. The susceptibility is highly temperature dependent. This is in agreement with a prediction due to Moriya and Kawabata, that in itinerant electron systems, close to the onset of magnetism, the renormalization of the magnetic susceptibility by electron correlations, leads to a Curie-like behavior.

DOI: 10.1103/PhysRevLett.109.197204 PACS numbers: 75.20.−g, 75.10.Lp, 75.30.Cr

Despite the fact that the *d* electronic shell is incomplete, none of the metallic elements from the 4*d* and the 5*d* series present ordered magnetic phases. The *d* band width is significantly larger than in the 3*d* series and the density of states at the Fermi level, $N(E_F)$ is consequently weaker. The conditions for the existence of stable magnetism (the Stoner criterion in a simple picture) are not satisfied. Some of the 4*d* and 5*d* metals, however, are close to the conditions for the onset of magnetism. The 4*d* metals Ru, Pd, or Rh, exhibit enhanced Pauli paramagnetism [1,2] with room temperature susceptibility reaching 8.0×10^{-4} for Pd and 1.6×10^{-4} for Rh and giant moments are found to develop on the 4*d* impurity atoms of dilute alloys with Fe or Co [3,4].

A number of theoretical studies predicted [5–11] that when 4*d* noble metals are prepared in the form of very small clusters (typically containing less than 50 atoms), stable ferromagnetism should be stabilized, due to band narrowing in low dimensions. By measuring the in-flight deflection of such very small clusters, Cox *et al.* [12] found that Rh clusters were ferromagnetic, whereas Pd and Ru clusters were not. The Rh intrinsic magnetic moment (''internal moment'' in Ref [12]), derived from these experiments, decreased with increasing the cluster size, from 0.8 μ_B/atom in 10-atom clusters to 0.1 μ_B/atom in 35-atom clusters. A magnetic moment of the same order of magnitude was found under an applied magnetic field of 5 T, for quasifree clusters, deposited or embedded in Ar [13].

From the above experiment, it was inferred that the stable moment on Rh disappears at cluster size above typically 100 atoms [12,13]. At larger cluster sizes, corresponding to 100–300 atoms, the type of magnetism encountered remains to be analyzed [14,15]. Indeed, the properties of correlated electron systems close to the onset of magnetism, is one of the fundamentally less-understood aspects of magnetism [16]. However, the realization of such studies has been hindered by experimental difficulties inherent to the experimental characterization of weakly magnetic systems. In the present study, we exploit the unique possibilities offered by x-ray magnetic circular dichroism (XMCD), specifically high sensitivity and element selectivity, to unambiguously detect the Rh magnetic signals in clusters.

The clusters were prepared by ion implantation within an Al_2O_3 matrix. The insulating nature of the matrix ensures that the electronic states within the Rh metallic clusters (equivalent to the Bloch states in an infinite periodic system) are confined to the cluster itself and do not extend into the matrix. Band narrowing, associated with electron confinement, tends to favor the onset of magnetic behaviors. A 90 nm-thick alumina film was deposited by atomic layer deposition (ALD) on a 25 μm thick kapton foil. A beam of negative Rh^- ions was used for implantation, produced from a NEC SNICS source [17]. The SNICS was operated at a high potential and the extracted negative ions were accelerated to 26 keV. The total incident dose reached 3.2×10^{16} Rh/cm^2. The major contamination of the beam reaching the irradiation chamber was due to RhO^- ions and it was estimated to be in the ppm range or lower. The expected Rh implanted depth profile was evaluated using the simulation code SRIM-2011 [18] (see Supplemental Material [19]). A more realistic profile of implanted Rh atoms was obtained after considering that the sample surface is progressively sputtered as implantation develops. The number of implanted atoms then amounts to 1.5×10^{16} and they are essentially distributed in the first 5 nm from the surface (see Supplemental Material [19]). From previous experiments dealing with the implantation of noble metals, such as Ag or Au within Al_2O_3 [20], it was expected as well that at the total implantation dose of

3.2×10^{16} Rh^-/cm^2, the Rh atoms will coalesce into clusters.

TEM studies (Fig. 1) were carried out on a freshly implanted sample, prepared in the same manner as the one studied by XMCD but deposited onto the carbon membrane of a copper-based TEM grid. The high angle annular dark field (HAADF) images were taken in STEM mode using a probe Cs-corrected FEI Titan 80–300 microscope operated at 200 kV. The bright field (BF) images were taken with a Philips CM300 microscope. As it can be seen from both HAADF and BF images, the observed Rh clusters exhibit an approximately spherical shape and are distributed densely and uniformly within the Al_2O_3 matrix (Fig. 1). The BF image in Fig. 1(b) taken at a higher magnification reveals that the clusters are essentially separated (see online additional information), with an average intercluster distance around 0.7 nm. The observed cluster separation corresponds to expectation since the clusters density here is only ~20% of the Rh full density and the characteristic feature of ion implantation is that it favors the formation of spherical and separated clusters (see Supplemental Material [19]). Assuming that the size distribution is Gaussian, the mean cluster diameter is 1.6 nm with a full width at half maximum of 0.7 nm (inset to Fig. 1). The cluster diameter corresponding to the highest occupancy probability is 1.8 nm. In addition, rare cluster agglomerates were found, representing less than 1% of the sample volume and having a diameter of about 5 nm. Note that the distribution of cluster size revealed by TEM has nearly no influence on the qualitative analysis presented below. Based on the previous studies of in-flight Rh clusters, the possible contribution of very small ferromagnetic clusters is expected to be negligible and the distribution in size over the nonferromagnetic clusters (see below) may affect the results quantitatively but not qualitatively.

Elemental analysis (see Supplemental Material [19]) was also performed using energy-dispersive x-ray spectroscopy analysis on a Philips CM300 microscope. No other element than rhodium, aluminum, and oxygen (from Al_2O_3 matrix), or carbon and copper (from the TEM grid) was found.

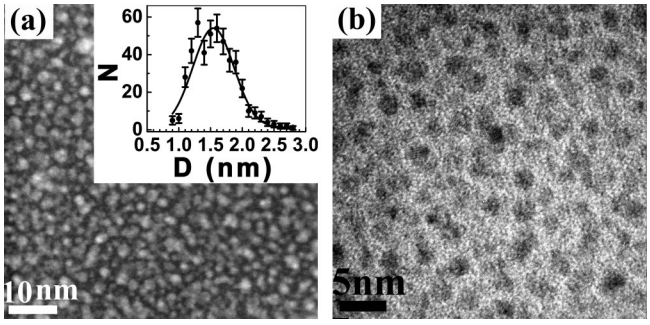

FIG. 1. (a) Dark field STEM image and (b) bright field image of the Rh clusters implanted in an Al_2O_3 matrix. Inset: experimental cluster size distribution (N = number of clusters, D = cluster diameter) and associated Gaussian fit.

No lattice fringe was observed which was attributed to the excessive thickness of the TEM lamella (70–80 nm thick). Lattice fringes were found in a sample which was implanted onto a 40 nm thick Al_2O_3 matrix at a lower implantation dose of 2×10^{16} Rh^-/cm^2, establishing the crystalline nature of the clusters in this case. These Rh clusters have a smaller size (1.3 nm) than in the higher dose sample object of the present study. According to experimental observations [21] and *ab initio* calculations [22], the critical volume above which the fcc bulk crystal structure is recovered is about 50 atoms. From this, it can be concluded that the Rh clusters examined by XMCD are crystalline.

The x-ray-absorption near-edge structure (XANES) and XMCD spectra of the clusters, at the Rh $L_{2,3}$ absorption edges, were measured at the ESRF beam line ID12. The first harmonic of the helical undulator HELIOS II was used to provide circularly polarized x rays in the energy range between 3.0 and 3.2 keV. At these energies, the Bragg angle of the Si⟨111⟩ double crystal monochromator is close to the Brewster angle of 45°. This leads to a strong reduction of the circular polarization rate of the x-ray beam, down to 12% and 5% at the L_2 and L_3 edges of Rh, respectively. The XANES spectra were recorded in the total fluorescence yield detection mode, using Si photodiodes. The XMCD spectra were obtained as the direct difference of the XANES spectra recorded with the helicity either antiparallel or parallel to the magnetic field applied to the sample. To eliminate possible experimental artifacts, the XMCD spectra were measured for two opposite directions of the applied magnetic field. The spectra were corrected for the incomplete circular polarization rate. The XMCD was measured at two different temperatures, 2.3 and 10 K. The magnetic field (B) up to 17 T, was produced by a superconducting solenoid (Cryogenics, Ltd). For the sake of data comparison, XMCD measurements were also performed at room temperature and $B = 2$ T, at the Rh $L_{2,3}$ edges on a 100 nm-thick ferromagnetic FeRh film.

The XANES spectrum of the Rh clusters and that of the FeRh thick film (Fig. 2), similar to those previously published [23,24], reveal characteristic differences. A strong reduction of the white line intensity is found in FeRh. It is ascribed to charge transfer from the Fe atoms to the Rh ones, as found in Rh-Pt alloys [25]. In contrast, the white line intensity obtained with the Rh clusters is similar to the one characterizing Rh metal (not shown) and no energy shift exists between both XANES spectra. These results indicate that the hybridization between the electronic states of the Rh clusters and the electronic states of the Al_2O_3 matrix is weak.

In contrast to the XANES spectra, the XMCD spectra of the Rh clusters (at 2.3 K and under 17 T) and of the FeRh film are quite similar in spectral shape (but not in intensities). To derive the spin and orbital moments carried by the Rh 4*d* electrons, the so-called magneto-optical

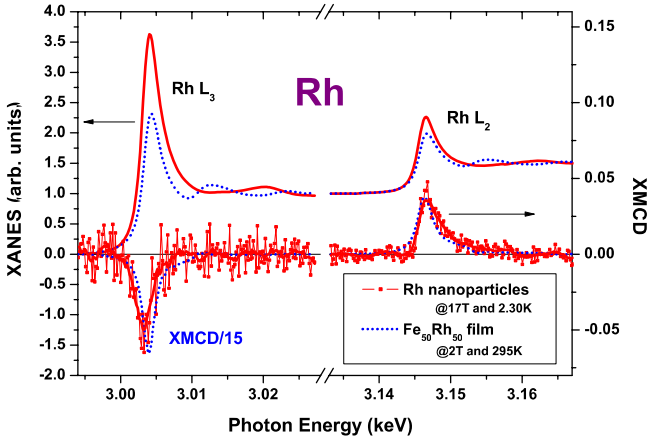

FIG. 2 (color online). Rh $L_{2,3}$ XANES and XMCD spectra measured on the Rh clusters (in red) and on a $Fe_{50}Rh_{50}$ film (dotted, in blue). The XMCD spectra are corrected for incomplete circular polarization rate. For the sake of comparison the XMCD signals recorded on a $Fe_{50}Rh_{50}$ film are divided by a factor of 15. The difference in spectral shape and amplitude is clearly visible at the Rh L_3 edge.

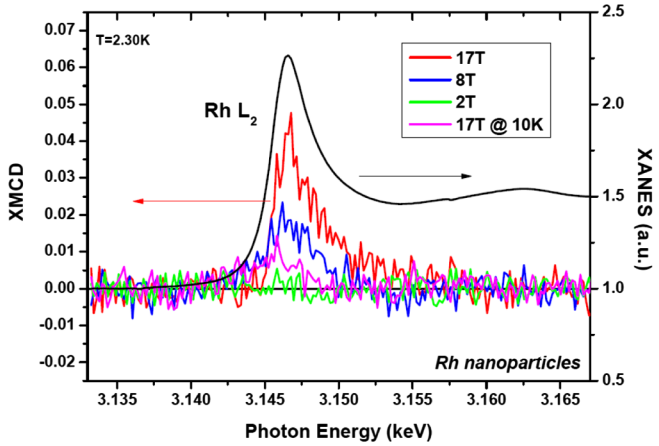

FIG. 3 (color online). XANES (in black) and XMCD signals at the L_2 edge measured on the Rh clusters under the different experimental conditions.

sum rules were applied to the experimental XMCD spectra [26,27]:

$$\langle S_z \rangle = \tfrac{3}{2}(A_3 - 2A_2)(n_{4d}/\sigma_{\mathrm{tot}}) - \tfrac{7}{2}\langle T_z \rangle \qquad (1)$$

and

$$\langle L_z \rangle = 2(A_3 + A_2)(n_{4d}/\sigma_{\mathrm{tot}}). \qquad (2)$$

In these relations, A_2 and A_3 are the integrated XMCD signals at the L_2 and L_3 edges, respectively, n_{4d} is the number of holes in the Rh $4d$ bands, σ_{tot} is the total absorption cross-section corresponding to $2p$-$4d$ transitions, and T_z is the spin magnetic dipole operator.

In the analysis, the contribution of the spin magnetic dipole $\langle T_z \rangle$ was neglected [24,28]. Even though this term is significant, it has the same field and temperature dependence as the total moment. Therefore its omission does not affect the main conclusions of the analysis. Following the standard procedure [28], the normalized x-ray absorption cross section per $4d$ hole, $r = n_{4d}/\sigma_{\mathrm{tot}} = 0.144$, was determined by subtracting the Ag-foil $L_{2,3}$ spectra from the experimental Rh $L_{2,3}$ spectra measured on the FeRh film and taking the theoretical value for the number of Rh $4d$ holes ($= 2.34$) from [29].

Using this value, the Rh $4d$ spin and orbital magnetic moments were derived. For FeRh, the spin and orbital moments are parallel to each other and are equal to $1.068 \pm 0.008\ \mu_{\mathrm{B}}$ and $0.070\ \mu_{\mathrm{B}} \pm 0.003\ \mu_{\mathrm{B}}$, respectively. This gives an orbital to spin ratio of the order of 0.06. Using exactly the same procedure for the Rh clusters, the average magnetic moment per Rh atom at 2.3 K and under 17 Tesla is equal to $0.067\ \mu_{\mathrm{B}} \pm 0.002\ \mu_{\mathrm{B}}$. Surprisingly the orbital contribution is very small, not exceeding 2% of the spin moment. The larger absolute errors in the moment values in FeRh compared to the Rh clusters, are due to the contribution of the magnetic EXAFS to the $L_{2,3}$ XMCD signals.

To unravel the origin of the Rh magnetic moment in the clusters, temperature, and field dependent measurements of the XMCD signal at the Rh L2-edge (8 and 2 T at 2.3 K and 17 T at 10 K) were performed. The signals shown in Fig. 3 have all the same spectral shape. Since the orbital moment was found negligibly small, at 2.3 K, the observed field and temperature dependence were assumed to reflect changes in the Rh $4d$ spin moment. The data are summarized in Table I.

The Rh spin moment derived at 2.3 K, varies linearly with the applied magnetic field (Fig. 4). From 2.3 to 10 K, the Rh moment measured under 17 T decreases by a factor of 3.5. The moment of $0.067\ \mu_{\mathrm{B}}$ measured at 2.3 K under 17 T is 20 times larger than the magnetic moment of $2.7 \times 10^{-4}\ \mu_{\mathrm{B}}$ expected from the known Pauli paramagnetic susceptibility of bulk rhodium [2]. Further, the Rh bulk susceptibility increases by about 7% from 0 to 300 K. In contrast, the strong decrease from 2.3 to 10 K, in the value of the Rh magnetic moments measured under 17 T mimics the behavior of an assembly of (super)paramagnetic uncoupled moments.

The finite temperature moment, μ_T, of an assembly of classical moments is expressed as

$$\mu_T = \mu_0 \mathcal{L}(x). \qquad (3)$$

TABLE I. Rh spin moment, M_s^{XMCD}, derived from XMCD data, and Rh spin moment M_s^{calc} calculated in a local moment picture, assuming a Rh localized moment of $0.2\ \mu_{\mathrm{B}}$.

$T(K)$, $B(T)$	2.3 K, 2 T	2.3 K, 8 T	2.3 K, 17 T	10 K, 17 T
M_s^{XMCD} (μ_{B})	0.002 (2)	0.029 (2)	0.067 (2)	0.019 (2)
M_s^{calc} (μ_{B})	0.008	0.032	0.065	0.015

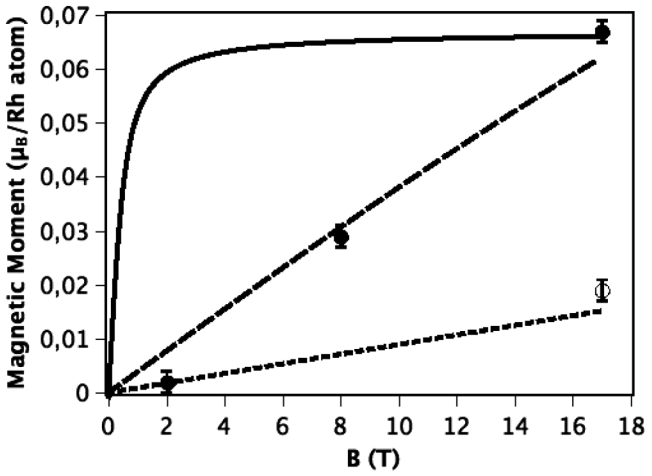

FIG. 4. Rhodium spin moment derived from XMCD measurements at 2.3 K (bold circles) and 10 K (open circle). Continuous line: calculated magnetization variation as a function of applied field at 2.3 K assuming clusters bearing a moment of 15 μ_B. Dashed line: calculated magnetization variation as a function of applied field B at 2.3 K (dashed line) and 10 K (dotted line) assuming Rh atoms bearing a local paramagnetic moment of 0.2 μ_B.

The 0 K moment of a given entity (atom or cluster), μ_0, is equal to $n\mu_{Rh}$, where n is the number of atoms in a given entity and μ_{Rh} is the Rh magnetic moment, $\mathcal{L}$ is the Langevin function, and $x = \mu_0 B/k_B T$. Based on previous studies [12,13], the possible occurrence of superparamagnetic clusters was considered first. From TEM observations, the number of atoms in a 1.8 nm–diameter cluster was derived to be $n \approx 220$. Since the Rh moment under 17 T at 2.3 K is of 0.067 μ_B/Rh, the moment of a given cluster μ_0 should be 15 μ_B or more. Then, the calculated magnetization at 2.3 K (as well as at 10 K), is nearly saturated above 5 T in complete disagreement with the experimental results (see Fig. 4). This discrepancy suggests that the Rh moments in a cluster are paramagnetic rather than ordered ferromagnetically. A satisfactory fit to the experimental data is obtained for $\mu_{Rh} = 0.2$ μ_B (Table I and Fig. 4).

However, the occurrence of uncoupled local moments is very unlikely for such a system of 4d itinerant electrons. Moriya [30] has shown that the models developed to describe the properties of very weak ferromagnets [31,32] should apply close to the onset of ferromagnetism. The susceptibility in these systems is strongly enhanced by exchange interactions. As temperature is increased, the enhancement factor is reduced due to the stiffening of spin fluctuations. The resulting temperature dependent paramagnetic susceptibility has been calculated in a primitive model, assuming an electron gaslike band structure. At sufficiently high temperature, the susceptibility displays a Curie-like behavior [30]. The main parameter in the calculation is the Stoner parameter $\alpha = Un(E_F)$ where $n(E_F)$ is the electron density at the Fermi level E_F, and U represents the exchange interactions between two electrons with opposite spins. The Stoner criterion for the onset of magnetism is given by $\alpha > 1$. For $\alpha = 0.992$, the low temperature susceptibility is enhanced by a factor 50 with respect to the free electron Pauli susceptibility (see Fig. 2 in Ref. [30]). In the present study, the enhancement factor with respect to the experimental Rh susceptibility amounts to 20. Considering the simplicity of the model and the fact that the parameter α is not well known, the qualitative agreement obtained can be considered satisfactory. The temperature dependent reciprocal susceptibility should deviate from linearity at low temperature, typically below $T/T_0 = 0.01$, where T_0 is the Curie temperature in the Stoner model, neglecting correlations (see [30]). Assuming $T_0 = 1000$ K, deviation should occur below 10 K. The ratio between the moments measured at 2.3 and 10 K under 17 T, equal to 3.5 (1.0), differs from the temperature ratio which amounts to 4.3. Although not statistically significant, this difference may be related to the expected saturation of the susceptibility at low T.

These results can be examined in the context of the existing band structure calculations, for Rh clusters containing up to 200 atoms, performed in the tight binding approach (Guirado-Lopez *et al* [33] and Barreteau *et al.* [6]). Above 100 atoms, the Rh magnetic moment is zero or very small. Because of the small number of atoms in a given cluster, the local density of states vary from one atom to another and the Stoner criterion may be locally fulfilled. Qualitatively, one may expect that such intrinsically heterogeneous magnetic state could favor the development of spin fluctuations. Unfortunately, even a semiquantitative description of these is not yet accessible to electronic structure calculations.

The weakness of the orbital moment is another characteristic feature emerging from the present study. One would expect the orbital moment to be larger in Rh, a 4d element, than in the 3d elements, Fe or Co. Most generally, the main contribution to the orbital moment is due to spin-orbit mixing between states close to the Fermi level E_F. In the present system, due to spin fluctuations, the splitting of the 4d band differs from one atom to another and, with this, the symmetry of the states close to E_F. Averaging over the contributions of each atom is expected to lead to a strong reduction of the total orbital moment. Additionally, the magnetism of the Rh clusters is expected to be essentially brought by Rh surface atoms (for which the electronic structure differs most from Rh bulk electronic structure). In the case of CoRh clusters, Muñoz-Navia *et al.* [34] found that the orbital moment carried by the Rh atoms at the cluster surface is negligibly small. Note that, due to the quenching of the orbital moment, no energy gap is expected in the excitation spectrum. This may favor the development of the here found spin fluctuations, in particular, at low temperature.

In conclusion, XMCD studies of Rh clusters obtained by ion implantation into an Al_2O_3 matrix reveal exchange-enhanced Pauli paramagnetism. The induced spin moment (0.067 μ_B at 2.3 K under 17 T) is approximately 20 times larger than in bulk Rh under the same experimental conditions. The spin moment is much larger than the orbital moment. This study constitutes an experimental confirmation of the fact that the renormalization of the magnetic susceptibility, due to electron correlations, leads to temperature dependent Curie-like behavior. Experimental difficulties had prevented earlier confirmation of this theoretical prediction.

[1] F. E. Hoare and J. C. Matthews, Proc. R. Soc. A **212**, 137 (1952).
[2] W. D. Weiss and R. Kohlhaas, Z. Angew. Phys. **23**, 175 (1967).
[3] A. M. Clogston, B. T. Matthias, M. Peter, H. J. Williams, E. Corenzwit, and R. C. Sherwodd, Phys. Rev. **125**, 541 (1962).
[4] R. M. Bozorth, H. J. Williams, and D. E. Walsh, Phys. Rev. **103**, 572 (1956).
[5] B. V. Reddy, S. N. Khanna, and B. I. Dunlap, Phys. Rev. Lett. **70**, 3323 (1993).
[6] C. Barreteau, R. Guirado-Lopez, D. Spanjaard, M. C. Desjonqueres, and A. M. Oles, Phys. Rev. B **61**, 7781 (2000).
[7] E. K. Parks, L. Zhu, J. Ho, and S. J. Riley, J. Chem. Phys. **100**, 7206 (1994).
[8] Yang Jinglong, F. Toigo, and W. Kelin, Phys. Rev. B **50**, 7915 (1994).
[9] C. M. Chang and M. Y. Chou, Phys. Rev. Lett. **93**, 133401 (2004).
[10] Young-Cho Bae, Hiroki Osanai, Vijay Kumar, and Yoshiyuki Kawazoe, Phys. Rev. B **70**, 195413 (2004).
[11] F. Aguilera-Granja, J. M. Montejano-Carrizalez, and R. A. Guirado-López, Phys. Rev. B **73**, 115422 (2006).
[12] A. J. Cox, J. G. Louderback, and L. A. Bloomfield, Phys. Rev. Lett. **71**, 923 (1993); A. J. Cox, J. G. Louderback, S. E. Apsel, and L. A. Bloomfield, Phys. Rev. B **49**, 12295 (1994).
[13] V. Sessi, K. Kuhnke, J. Zhang, J. Honolka, K. Kern, C. Tieg, O. Šipr, J. Minár, and H. Ebert, Phys. Rev. B **82**, 184413 (2010).
[14] G. H. Lee, Y. T. Jeon, S. H. Huh, B. KIm, J. Park and S. T. Oh, J. Korean Phys. Soc. **46**, 556 (2005).
[15] Y. T. Jeon and G. H. Lee, J. Appl. Phys. **103**, 094313 (2008).
[16] X. Xu, S. Yin, R. Moro, A. Liang, J. Bowlan, and W. A. de Heer, Phys. Rev. Lett. **107**, 057203 (2011).
[17] J. Ishikawa, Rev. Sci. Instrum. **79**, 02C506 (2008).
[18] J. F. Ziegler, M. D. Ziegler, and J. P. Biersack, Nucl. Instrum. Methods Phys. Res., Sect. B **268**, 1818 (2010).
[19] See Supplemental Material at http://link.aps.org/supplemental/10.1103/PhysRevLett.109.197204 for a description of cluster preparation, of TEM images, and of the energy-dispersive x-ray spectroscopy analysis.
[20] P. K. Kiuri, J. Appl. Phys. **108**, 054301 (2010).
[21] J. Evans and M. Tromp, J. Phys. Condens. Matter **20**, 184020 (2008).
[22] T. Futschek, M. Marsman and J. Hafner, J. Phys. Condens. Matter **17**, 5927 (2005).
[23] A. Smekhova, N. Atamena, D. Ciuculescu, P. Lecante, F. Wilhelm, C. Amiens, A. Rogalev, J. Phys. Conf. Ser. 200, 072091 (2010).
[24] J. Chaboy, F. Bartolomé, M. R. Ibarra, C. I. Marquina, P. A. Algarabel, A. Rogalev, and C. Neumman, Phys. Rev. B **59**, 3306 (1999).
[25] K. Siepen, H. Boennemann, W. Brijoux, J. Rothe, and J. Hormes, Appl. Organomet. Chem. **14**, 549 (2000).
[26] B. T. Thole, P. Carra, F. Sette, and G. van der Laan, Phys. Rev. Lett. **68**, 1943 (1992).
[27] P. Carra, B. T. Thole, M. Altarelli, and X. Wang, Phys. Rev. Lett. **70**, 694 (1993).
[28] J. Vogel, A. Fontaine, V. Cros, F. Petroff, J. P. Kappler, G. Krill, A. Rogalev, and J. Goulon, Phys. Rev. B **55**, 3663 (1997).
[29] C. Stamm, J.-U. Thiele, T. Kachel, I. Radu, P. Ramm, M. Kosuth, J. Minár, H. Ebert, H. A. Dürr, W. Eberhardt, and C. H. Back, Phys. Rev. B **77**, 184401 (2008).
[30] T. Moriya, J. Magn. Magn. Mater. **14**, 1 (1979).
[31] T. Moriya and A. Kawabata, J. Phys. Soc. Jpn. **34**, 639 (1973).
[32] K. K. Murata and S. Doniach, Phys. Rev. Lett. **29**, 285 (1972).
[33] R. Guirado-López, M. C. Desjonquères, and D. Spanjaard, Phys. Rev. B **62**, 13188 (2000).
[34] M. Muñoz-Navia, J. Dorantes-Dávila, D. Zitoun, C. Amiens, N. Jaouen, A. Rogalev, M. Respaud, and G. M. Pastor, Appl. Phys. Lett. **95**, 233107 (2009).